

MSEC2016-8693

THE COUPLING BETWEEN DENSIFICATION AND OPTICAL HEATING IN INTENSE PULSED LIGHT SINTERING OF SILVER NANOPARTICLES

Shalu Bansal

Department of Mechanical
Engineering,

Oregon State University

Corvallis, Oregon, USA

Chih-hung Chang

Department of Chemical
Engineering,

Oregon State University

Corvallis, Oregon, USA

Rajiv Malhotra

Department of Mechanical
Engineering,

Oregon State University

Corvallis, Oregon, USA

KEYWORDS

Intense Pulsed Light Sintering, Temperature, Densification

ABSTRACT

Sintering of nanoparticles deposited onto rigid or flexible substrate is required for many devices that use continuous and patterned thin films. An emerging need in this area is to perform nanoparticle sintering under ambient conditions at high speeds with throughput that is compatible with high speed nanoparticle deposition techniques. Intense Pulsed Light sintering (IPL) has the capability to meet this need. It uses high energy, broad area and broad spectrum beam of xenon lamp light to sinter metallic and non-metallic nanoparticles. This paper experimentally examines the temperature evolution and densification during IPL. It is shown for the first time that temperature rise and densification in IPL are related to each other. A coupled optical-thermal-sintering model on the nanoscale is developed to understand this phenomenon. This model is used to show that the change in the nanoscale shape of the nanoparticle ensemble due to sintering reduces the optically induced heating as the densification proceeds, which provides a better explanation of experimental observations as compared to current models of IPL. The implications of this new understanding on the performance of IPL are also discussed.

INTRODUCTION

Recently there has been a need for rapid and large area sintering of nanoparticles, deposited onto thermally tolerant and thermally sensitive substrates via various selective and broad area deposition techniques, into functional solid structures. Intense Pulsed Light sintering (IPL) or Photonic Sintering has generated significant interest as a process that can be used for the above purpose. IPL uses broad-spectrum, pulsed or continuous, light from a xenon lamp incident onto nanoparticles deposited on a substrate as shown in Figure 1. The incident optical energy is converted into heat by the nanoparticles resulting in rapid densification of the nanoparticles. The key advantage of photonic sintering over conventional nanoparticle sintering processes is faster densification of nanoparticle inks, about a few tens of seconds, over large area substrates (demonstrating an optical footprint of 0.75"x12" or greater) under ambient conditions [1-3]. It has been reported that IPL can minimize thermally induced damage to temperature sensitive substrates [4] and can increase adherence of the sintered nanoparticle film to the underlying substrate [5]. Due to the above qualities, IPL is amenable to integration with roll-to-roll and printing based techniques for high-speed and flexible manufacturing of the above devices [6]. IPL of both metallic and non metallic nanoparticle materials has been demonstrated for applications in RFID tags [4], solar cells [1, 7, 8] and flexible electronics [6, 9, 10].

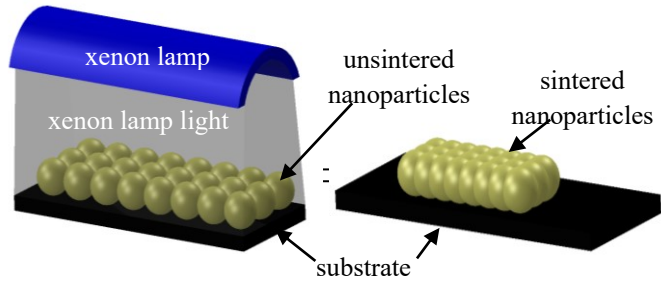


Figure 1: Schematic of IPL

Key process performance metrics in IPL include control of densification in the sintered nanoparticle film, along with minimal temperature rise of the underlying substrate and minimal sintering time. Critical process parameters that control these metrics are the energy per pulse of the incident light, number of pulses and duty cycle of pulses. Past work in IPL has experimentally examined the effect of the above parameters on densification. Increasing the number of exposures of the nanoparticles to the xenon lamp light increases the density of the sintered nanoparticles [3, 6, 9, 11]. However, beyond a certain number of exposures there is little further increase in the density. Increasing the light energy per exposure and the duration of the exposure also results in faster densification. Further, for a given optical power and exposure time, smaller nanoparticles result in higher density of the sintered material [10, 12].

Since the substrate temperature, sintered nanoparticle density and time required to achieve the desired density depend on the temperature rise in the nanoparticles, experimental characterization and modeling of temperature evolution during photonic sintering is necessary to control the process. West et al. [13] combined effective medium theory, with a thermal transfer model and known incident optical power, to model the interaction between heat generation at the surface and heat conduction into the bulk of the deposited nanoparticles. Kim et al. [14] measured light absorption by the as-deposited nanoparticles and combined it with known nanoparticle mass and incident optical power to predict nanoparticle melting. However, these works did not experimentally measure the actual temperature evolution during IPL, or compare it to theoretical predictions. Park et al. [15] experimentally measured the temperature rise and densification as a function of the IPL process parameters for PVP-coated Cu nanoparticles. A mesoscale heat transfer based model was developed that predicted the experimentally observed temperature evolution of the nanoparticles fairly well. However, the temperature measurement and modeling was performed for one pulse of incident light only. Further, the developed model assumed that all the incident optical energy was absorbed by the deposited nanoparticles. This precludes the known absorption efficiency of nanoparticles and the known variation in optical power output of a xenon lamp with wavelength.

This work quantifies temperature evolution and change in microstructure of silver nanoparticles deposited on a Polyamide substrate, during IPL. Silver nanoparticles are chosen since they are a well known conductive nanomaterial system that has been sintered extensively using IPL. The temperature evolution during IPL is measured, as a function of the incident energy per pulse and the number of pulses, using a thermal camera. The grain size and microstructural morphology of the sintered material are quantified using X-ray diffraction and Scanning Electron Microscopy. It is shown that contrary to current reports in literature the nanoparticle temperature does not increase monotonically during IPL, but drops significantly as densification progresses. A nanoscale coupled optical-thermal-sintering model is used to understand the fundamental physics behind this new experimental observation. Finally, the impact of this new understanding on the performance of IPL is discussed.

EXPERIMENTAL METHODS

Silver nanopowder of nominal diameter 20 nm, from US Research Nanomaterials, was suspended in tetradecane at 48 wt% of silver, to create silver nanoparticle ink. 100 microliters of the ink was deposited on Polyamide 6.6 substrate (25 mm x 19 mm and 250 μm thick), via spin coating at 800 rpm for 2 seconds. The deposited silver film was dried in ambient conditions for 24 hours. A Sinteron 3000-L flash lamp (Xenon Corp., USA) was used for IPL of the spin coated samples. The setup used (Figure 2) consisted of a controller which can regulate the critical lamp parameters, a 16 inch Xenon lamp, a sample mounting platform and a thermal camera to record temperatures of the deposited film during IPL. The spin coated samples were placed at a distance of 1.5 inch below the lamp window resulting in an optical footprint of 25.4 mm x 300 mm at the substrate. The IPL and lamp parameters which were varied during experiments are shown in Table 1.

A MicroEpsilon thermo-imager TIM-200 thermal camera that records temperatures upto 1500°C, with a maximum error of $\pm 2^\circ\text{C}$, spatial resolution of 96 pixels per inch and acquisition frequency of 128 Hz, was used to measure the film temperature during IPL. The camera was calibrated by heating the dried silver sample to a known temperature on a hot plate and setting the emissivity used by the camera to match the temperature set in the hot plate. The nominal thickness of the film was measured to be 8-10 μm , using Zemeteric Zscope white light interferometer. Wide angle X-ray diffraction (Bruker AXS D8 Discover) was used to examine the crystalline phase of the sintered and unsintered films. Scanning electron microscopy (SEM) of sintered and unsintered samples was performed using a FEI Quanta 3D machine.

Table 1: IPL parameters used in experiments

Voltage (kV)	Pulse on/off time (ms)	Number of pulses	Resultant energy per pulse (J)
2.2	0.250/121	50,90,150	48
2.5	0.260/143	50,90,150	68
2.8	0.255/160	50,90,150	88

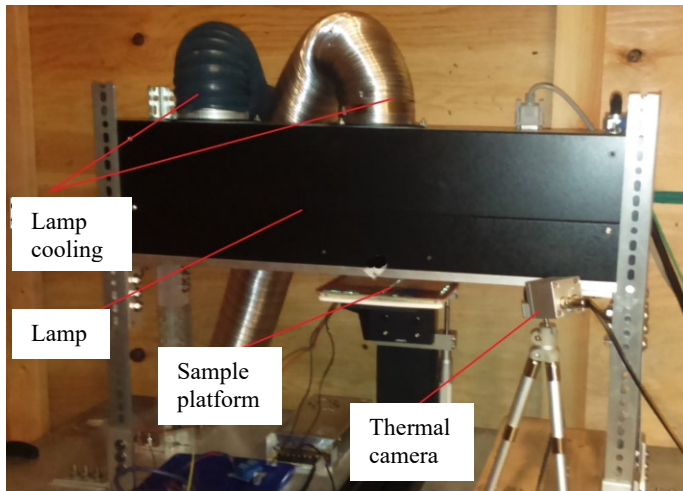


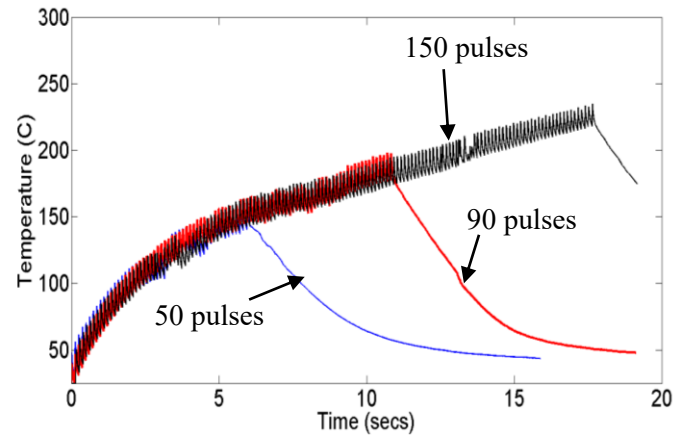
Figure 2: Experimental setup used for IPL

EXPERIMENTAL RESULTS

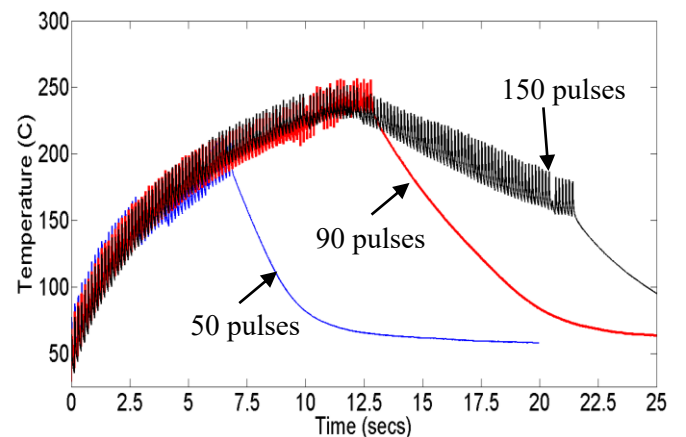
Figure 3 shows the temperature evolution of the nanoparticles for three different incident light energy levels with varying number of pulses. There is a significant decrease in temperature rise as the silver film reaches a temperature of around 250°C , which corresponds to around 90 pulses for incident energy of 68 J per pulse and 88 J per pulse. This indicates that for these two cases, after about 90 pulses, the thermal energy generated by the incident light is being surpassed by thermal losses. For the case of 48 J per pulse incident energy, the temperature rises continuously, but does not reach a temperature of 250°C for up to 150 pulses. It is worth noting that the temperatures recorded during IPL are not high enough to cause melting of the silver nanoparticles even after accounting for the size dependent depression in melting point of nanoparticles (Figure 3d, [16]). Figure 3 essentially illustrates that a critical amount of energy is required for densification to commence. This critical energy is the activation energy required for mass transfer and is specific to the microstructure obtained during the deposition process like spin

coating process in this work. Given that all samples were prepared the same way, it is expected that this activation energy is similar for all our samples. The supply of this activation energy to the nanoparticles raises its temperature to around 250°C which is the critical temperature for densification to begin. No temperature drop is seen in the case of 48 J energy per pulse because sufficient energy has not been delivered by the light to overcome the activation energy.

Figure 4 shows integrated intensity as a function of 2θ plots for the unsintered and sintered silver nanoparticles as obtained from Wide Angle X-ray diffraction. Figure 5 plots the intensity at the dominant (111) crystal orientation as a function of number of pulses and pulse energies. The increase in peak intensity of the sintered samples in Figure 4 indicates an increase in size of crystallites due to IPL. Increasing the number of pulses increases the crystallite size as shown in Figure 5 and also reported in past literature on IPL. Figure 5 also shows that the relative increase in peak intensities is much higher for the 68J and 88 J per pulse cases for any number of pulses, as compared to the 48 J per pulse case.



(a)



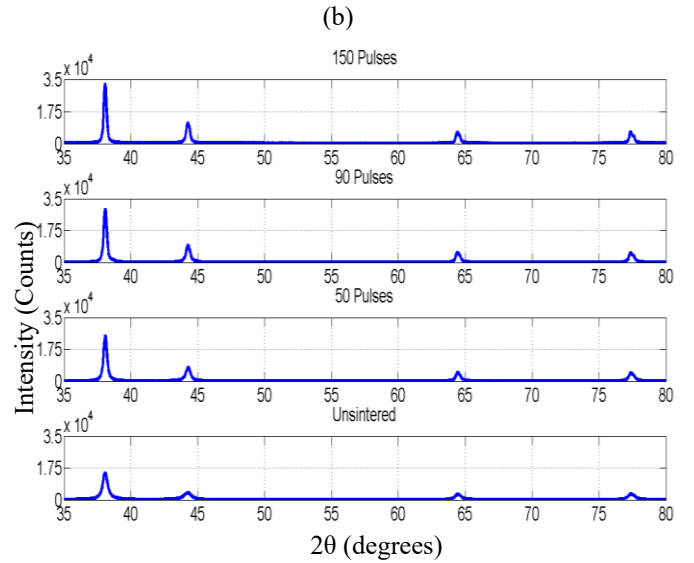
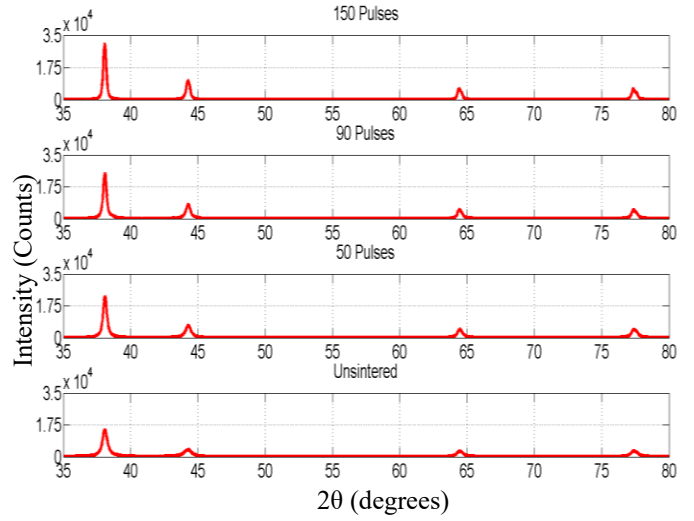
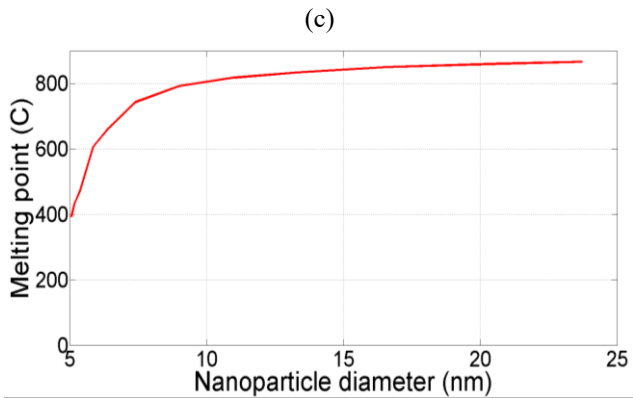
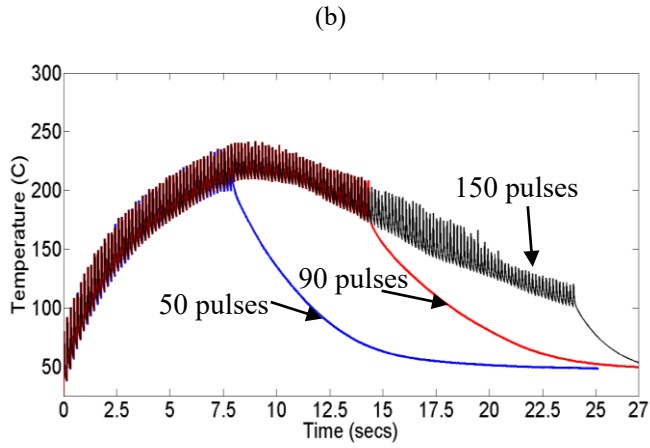


Figure 3: Temperature evolution for (a) 48 J per pulse (b) 68 J per pulse (c) 88 J per pulse and (d) melting point of silver nanoparticles as a function of nanoparticle diameter [16]

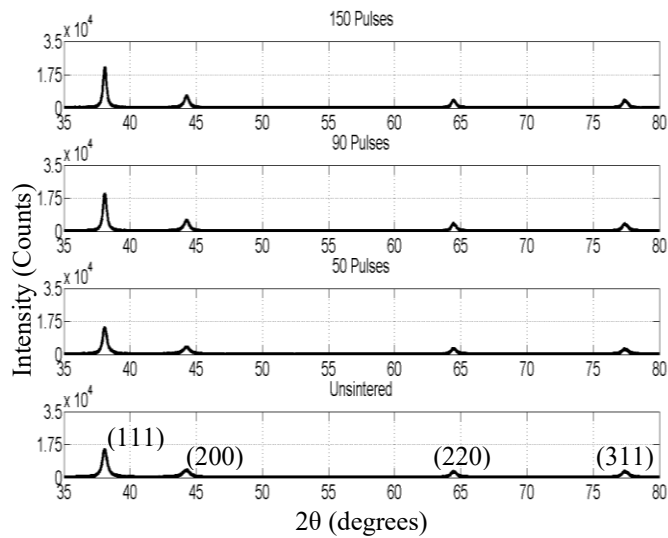


Figure 4: Integrated Intensity vs 2θ plots from XRD

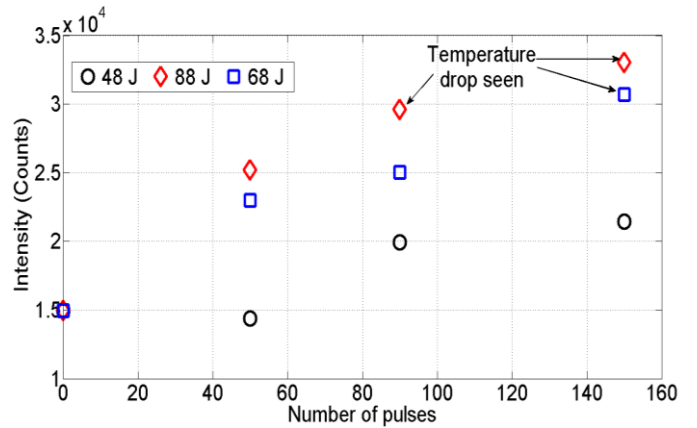
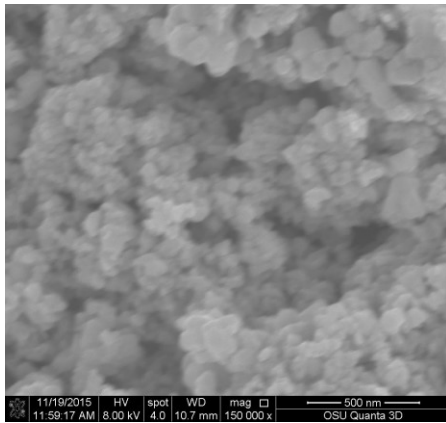
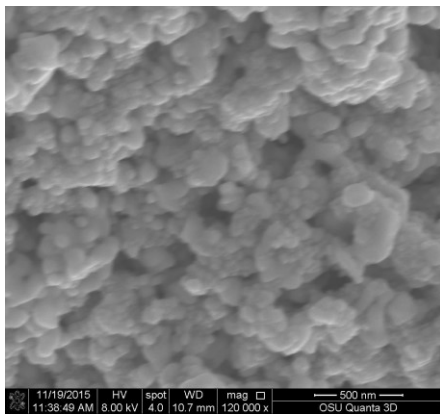


Figure 5: Integrated Intensity at orientation (111) for different number of pulses and pulse energies

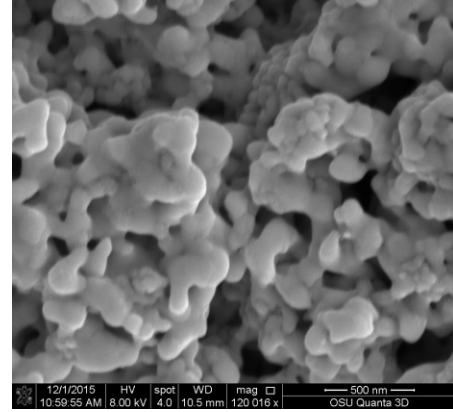
Figure 6 shows representative SEM images of the un-sintered and sintered nanoparticles for 150 pulses at different energies per pulse. The maximum and minimum Feret's diameter calculated from these SEM images using ImageJ software are shown in Figure 7. The Feret's diameter of an object in a given direction is the distance between the two parallel planes restricting the object perpendicular to that direction. In this case, the greater the Feret's diameter of the particles, the greater is the coalescence due to sintering between adjacent nanoparticles. Figure 7 shows that there is minimal growth of particle size for an energy of 48 J per pulse as compared to 68 J and 88 J per pulse. Examining the above experimental data as a whole shows that the drop in temperature of the film during IPL appears occurs when the degree of sintering between the nanoparticles reaches a critical point. The existence of this kind of critical point can be seen in Figure 5, since a drop in temperature is always observed as the particles reach a size corresponding to an intensity of around 30000 counts. Within our knowledge, this non-monotonic and densification-dependent nature of temperature evolution in IPL has not been shown before. The next section develops a model that can physically, if only qualitatively, explain this phenomenon.



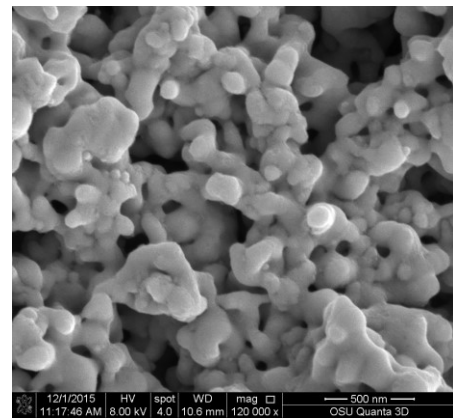
(a)



(b)



(c)



(d)

Figure 6: Representative SEM images of (a) un-sintered silver and sintered silver for 150 pulses for energy of (b) 48 J per pulse (c) 68 J per pulse (d) 88 J per pulse

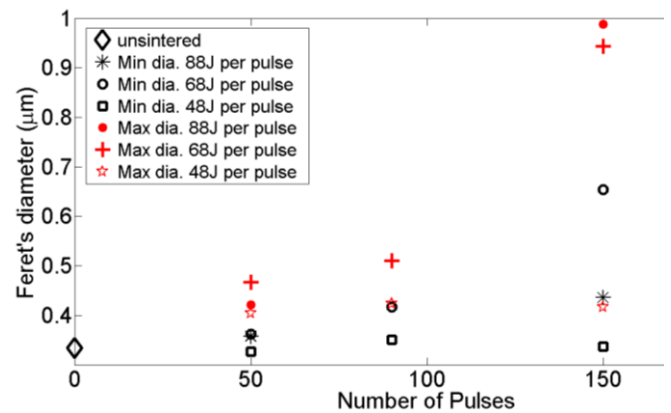


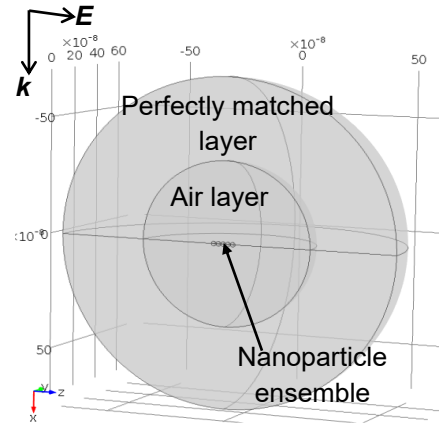
Figure 7: Feret's diameter of the sintered material as a function of incident light energy and number of pulses

COMPUTATIONAL MODELING

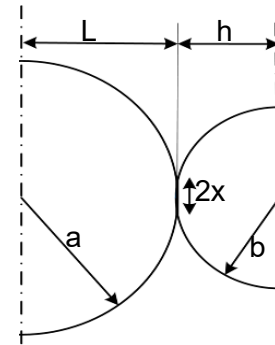
Past work by the authors developed a model [17] that couples optically induced heating and nanoscale mass transport, to predict temperature evolution and densification in an idealized row of equal-sized silver nanoparticles (Fig. 8a) that are subjected to continuous xenon lamp light. During densification without melting, mass transport between the nanoparticles causes neck growth between adjacent nanoparticles as well as a reduction in nanoparticle size, due to grain boundary diffusion and surface diffusion. The model developed in [17], used a full-field electromagnetic simulation in COMSOL FEA (Fig. 8b) to capture the effect of this change in ensemble shape on the optically-induced heat generation. The wavelength dependent dielectric constants of silver were obtained from the Drude-Lorentz model [18]. Equilibrium configurations of the nanoparticle ensemble were obtained using a McMeeking-Cocks-Suo model [19] in which geometric parameters (Fig. 8c) are used to quantify neck growth between adjacent nanoparticles. It can be noted that a greater value of x/b and a lower value of $(L+h)/(a+b)$ indicates greater degree of sintering between two adjacent nanoparticles. The FEA model was then used to quantify the optically induced heat generation Q as a function of the ratio x/b . The function Q vs. x/b was fed back into the McMeeking-Cock-Suo model along with the incident electric field, which corresponds to the incident energy per pulse while assuming the light is travelling in air, to calculate the evolution of temperature and the resultant densification in the nanoparticle ensemble. Conduction in the ensemble was neglected, since the size of the ensemble is very small which results in a significantly smaller thermal diffusion time as compared to the sintering time. Radiation losses from the ensemble were modeled using the Stefan-Boltzmann law with an emissivity of 0.07 for silver. The simulation was stopped when the value of x/b reached 0.9, since the McMeeking-Cocks-Suo model is thereafter not valid. An overall schematic of this framework, which was implemented in MATLAB via forward Euler integration, is shown in Fig. 8d. The reader is referred to reference [17] for more details on this modeling framework.



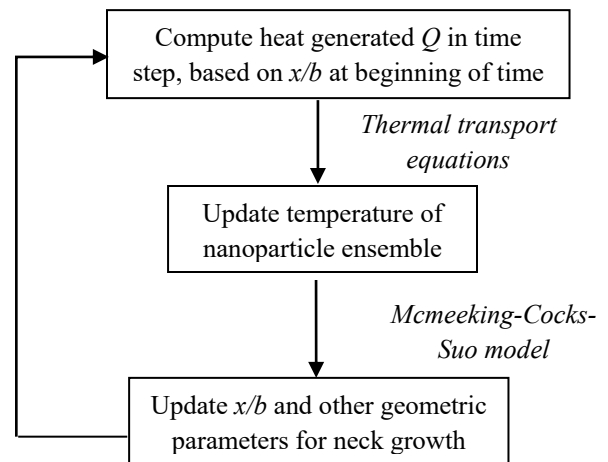
(a)



(b)



(c)



(d)

Figure 8: (a) Idealized nanoparticle system with E showing the direction of polarization of the incident wave and k showing the direction of propagation of the incident (b) COMSOL model used for full field simulations (c) Schematic of geometric parameters used in the McMeeking-Cocks-Suo model.

Figure 9 shows representative contour plots of optically-induced thermal heating obtained from the COMSOL simulations, for a chain of five 20 nm diameter nanoparticles, subjected to an electric field of 1 V/m at a wavelength of 400 nm. Figure 10 shows the corresponding total thermal power generated as a function of the incident wavelength λ , i.e. ζ , at different values of x/b . The total heat generated (Q) in the nanoparticle ensemble was obtained as a function of x/b according to equation (1) below.

$$\zeta = \frac{Q}{\lambda} \quad (1)$$

Where, for a given x/b , ζ corresponds to the curve shown in Figure 10, and ζ is obtained from the wavelength dependent relationship between the incident power ζ and the commanded power ζ as supplied by the xenon lamp manufacturer (Figure 11). Figure 12 shows the predicted evolution of temperature, and of the ratios x/b and $(L+h)/(a+b)$, for a continuous incident xenon lamp light of 68 J energy incident on the nanoparticle assembly for 5 seconds. Additionally, the same computational framework was also used to capture temperature rise and densification for the case where Q is uncoupled with x/b , by assuming that Q stays at the value corresponding to $x/b=0$ throughout the simulation.

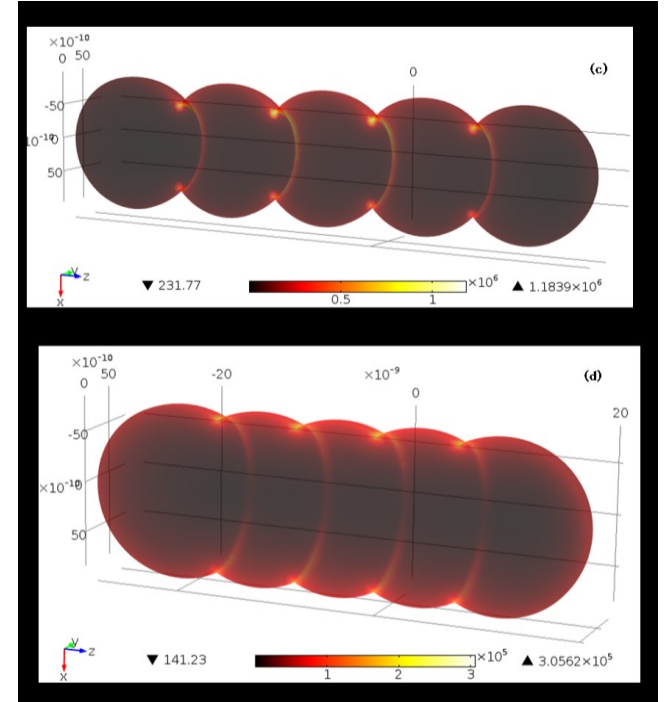
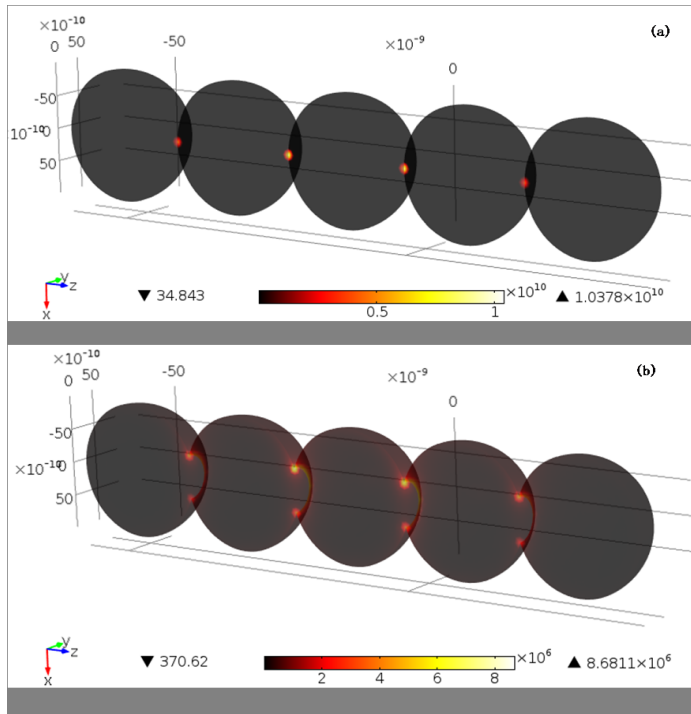


Figure 9: Contour plots of Thermal power density (in W/m^3) 1V/m incident field at 400 nm wavelength for (a) $x/b = 0$ (b) $x/b = 0.3$ (c) $x/b = 0.6$ (d) $x/b = 0.88$. Units on axis are in meters.

Figure 10: Total thermal power generated (in Watt) per unit incident optical power i.e. ζ

The comparison of predicted temperature evolution from the coupled and the uncoupled model in Figure 12a, shows that as compared to the coupled model a continuous temperature rise is predicted by the uncoupled model. Further the temperature rise is much higher and much faster in the uncoupled model as compared to the coupled model. In all, the

coupled model represents the rise and then drop in the temperature during IPL much better than the uncoupled model.

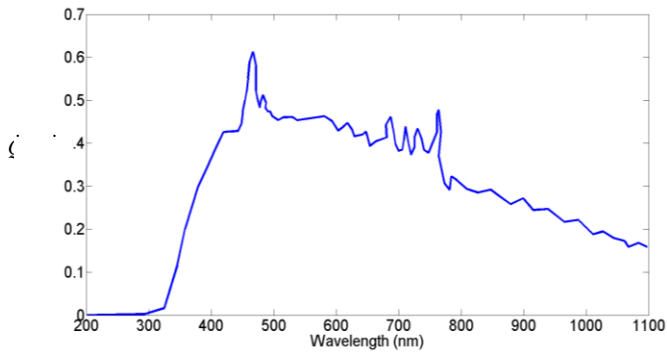
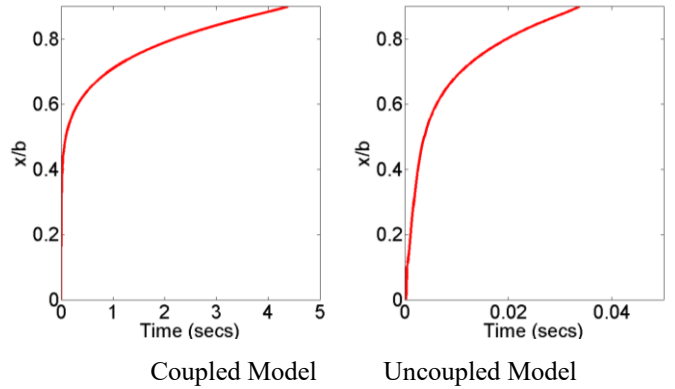
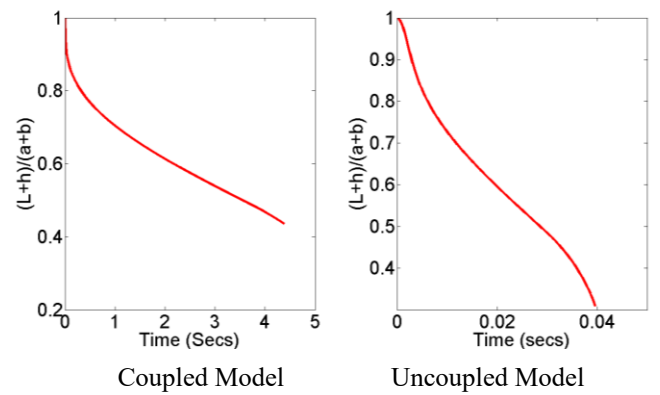


Figure 11: Dependence of the ratio of incident xenon lamp power to commanded lamp power, i.e., ζ as a function of the optical wavelength.

Examining the predicted x/b and $(L+h)/(a+b)$ in Figure 12b and 12c shows that the uncoupled model predicts much faster densification than the coupled model. The predicted evolution of optically induced heating and thermal losses from the nanoparticle system (Figure 13), with the coupled and the uncoupled models, shows that the drop in Q with the progress of densification is the key phenomenon that causes the drop in temperatures seen in Figs. 3b and 3c. Essentially the drop in optically induced heating due to change in nanoparticle shape, reduces the further heat that can be generated in the nanoparticle ensemble by the incident light, allowing thermal losses to overtake heat generation. This results in a reduction in temperature and a retardation in the rate of densification.

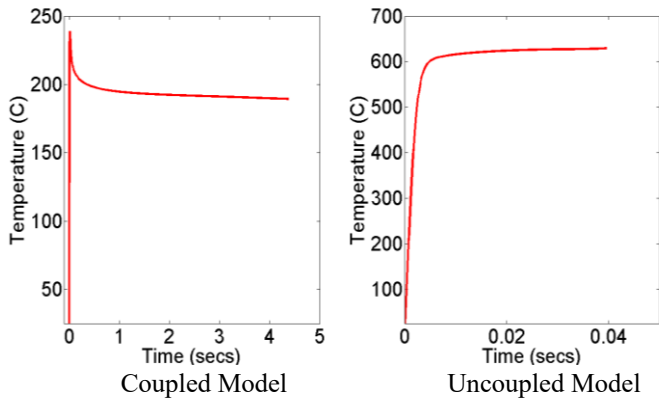


(b)



(c)

Figure 12: Comparisons between predictions of (a) nanoparticle temperature (b) ratio x/b and (c) ratio $(L+h)/(a+b)$ from the coupled and uncoupled models



(a)

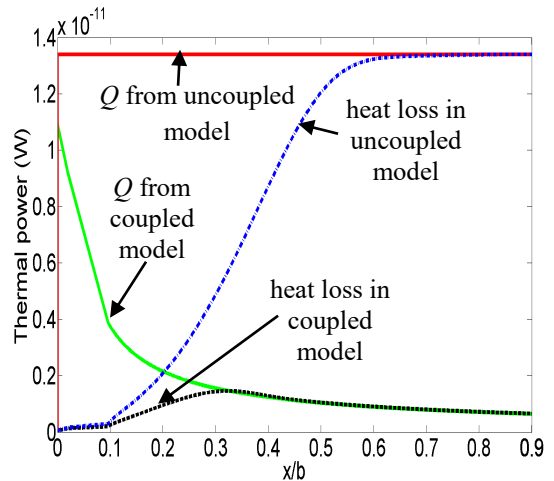


Figure 13: Comparisons of predicted optically induced heating vs. losses from the coupled and uncoupled models

In the uncoupled model, the assumption of constant optically induced heating cannot predict the temperature drop seen in experiments because the thermal losses take a longer time to catch up to the heat generation. Note that while the coupled model captures the experimentally observed trend of the temperature drop, the predicted temperature stabilizes to around 200°C as compared to a monotonic reduction in post-peak temperature seen in Figure 3(b) and 3(c). This is probably because the effects of thermal conduction into the substrate are not accounted for in the present model.

SUMMARY AND CONCLUSIONS

Understanding the evolution of temperature and concomitant densification of nanoparticles is critical to controlling the IPL process. This paper experimentally examines the above in IPL of metallic silver nanoparticles. It is shown for the first time that the temperature rise in IPL is of a non-monotonic nature and the temperature evolution is connected to the evolution of sintering between the nanoparticles. Additionally, a coupled model developed by the authors in past work is used to understand that the root cause behind this phenomenon is that the change in nanoparticle shape due to sintering alters the optical response of the nanoparticle ensemble. This understanding can lead to more accurate simultaneous control of densification, temperature rise of the substrate and throughput in IPL, in the near future. Our future work will focus on developing a mesoscale model for IPL that accounts for the phenomenon observed here.

ACKNOWLEDGMENTS

The authors gratefully acknowledge the support from the National Science Foundation grant number CMMI#1537196 for this work.

REFERENCES

- Galagan, Y., Coenen, E. W. C., Abbel, R., Van Lammeren, T. J., Sabik, S., Barink, M., Meinders, E. R., Andriessen, R., and Blom, P. W. M., *Photonic sintering of inkjet printed current collecting grids for organic solar cell applications*. *Organic Electronics*, 2013. **14**(1): p. 38-46.
- Niittynen, J., Sowade, E., Kang, H., Baumann, R. R., and Mantysalo, M., *Comparison of laser and intense pulsed light sintering (IPL) for inkjet-printed copper nanoparticle layers*. *Sci. Rep.*, 2015. **5**.
- Niittynen, J., Abbel, R., Mäntysalo, M., Perelaer, J., Schubert, U. S., and Lupo, D., *Alternative sintering methods compared to conventional thermal sintering for inkjet printed silver nanoparticle ink*. *Thin Solid Films*, 2014. **556**(0): p. 452-459.
- Bjorninen, T., Virkki, J., Sydanheimo, L., and Ukkonen, L., *Manufacturing of antennas for passive UHF RFID tags by direct write dispensing of copper and silver inks on textiles*. in *Electromagnetics in Advanced Applications (ICEAA), 2015 International Conference on*. 2015.
- Joo, S.-J., Park, S.-H., Moon, C.-J., and Kim, H.-S., *A highly reliable copper nanowire/nanoparticle ink pattern with high conductivity on flexible substrate prepared via a flash light-sintering technique*. *ACS Applied Materials & Interfaces*, 2015. **7**(10): p. 5674-5684.
- Hosel, M. and Krebs, F. C., *Large-scale roll-to-roll photonic sintering of flexo printed silver nanoparticle electrodes*. *J. Mater. Chem.*, 2012. **22** p. 15683-15688.
- Dhage, S. R., Kim, H. S., and Hahn, H. T., *Cu(In,Ga)S₂ thin film preparation from a Cu(In,Ga) metallic alloy and Se nanoparticles by an intense pulsed light technique*. *Journal of Electronic Materials*, 2011. **40**(2).
- Lee, J. H., Lee, Y. M., Lim, S. J., Choi, D. K., and Yu, J.-W., *Intense pulsed light annealed buffer layers for organic photovoltaics*. *Solar Energy Materials and Solar Cells*, 2015. **143**: p. 517-521.
- Kang, K., Sowade, E., and Baumann, R. R., *Direct intense pulsed light sintering of inkjet-printed copper oxide layers within six milliseconds*. *ACS Appl. Mater. Interfaces*, 2014. **6**: p. 1682-1687.
- Lee, D. J., Park, S. H., Jang, S., Kim, H. S., Oh, J. H., and Song, Y. W., *Pulsed light sintering characteristics of inkjet-printed nanosilver films on a polymer substrate*. *J. Micromech. Microeng.*, 2011. **21**.
- Wang, B. Y., Yoo, T. H., Song, Y. W., Lim, D. S., and Oh, Y. J., *Cu ion ink for a flexible substrate and highly conductive patterning by intensive pulsed light sintering*. *ACS Appl. Mater. Interfaces*, 2013. **5**: p. 4113-4119.
- Hwang, H.-J., Chung, W.-H., and Kim, H.-S., *In situ monitoring of flash-light sintering of copper nanoparticle ink for printed electronics*. *Nanotechnology*, 2012. **23**(48).
- West, J., Carter, M., Smith, S., and Sears, J., *Photonic Sintering of Silver Nanoparticles: Comparison of Experiment and Theory*, in *Sintering Methods and Products*, D.V. Shatokha, Editor 2012, InTech. p. 173-188.
- Kim, H.-S., Dhage, S., Shim, D.-E., and Hahn, H. T., *Intense pulsed light sintering of copper nanoink for printed electronics*. *Applied Physics A*, 2009. **97**(4): p. 791-798.
- Park, S.-H., Chung, W.-H., and Kim, H.-S., *Temperature changes of copper nanoparticle ink during flash light sintering*. *Journal of Materials Processing Technology*, 2014. **214**(11): p. 2730-2738.

16. Alarifi, H. A., Atiş, M., Özdoğan, C., Hu, A., Yavuz, M., and Zhou, Y., *Determination of complete melting and surface premelting points of silver nanoparticles by molecular dynamics simulation*. The Journal of Physical Chemistry C, 2013. **117**(23): p. 12289-12298.
17. Macneill, W., Choi, C.-H., Chang, C.-H., and Malhotra, R., *On the self-damping nature of densification in photonic sintering of nanoparticles*. Scientific Reports, 2015. **5**: p. 14845.
18. Fan, X., Zheng, W., and Singh, D. J., *Light scattering and surface plasmons on small spherical particles*. Light: Science & Applications, 2014. **3**.
19. Parhami, F., Mcmeeking, R. M., Cocks, A. C. F., and Suo, Z., *A model for the sintering and coarsening of rows of spherical particles*. Mechanics of Materials, 1999. **31**(1): p. 43-61.